RNA helicase DHX15 exemplifies a unique dependency in acute leukemia

Hao Guo,[1,2,3*] Jin Xu,[1,2*] Peiqi Xing,[4*] Qilong Li,[1,2] Donghai Wang,[1,2] Chao Tang,[5] Bruno Palhais,[6] Juliette Roels,[6] Jiaxu Liu,[1,2] Sa Pan,[1,2] Jinyan Huang,[7] Zhaoqi Liu,[4] Ping Zhu,[5] Tom Taghon,[8] Guoliang Qing,[2] Pieter Van Vlierberghe[6] and Hudan Liu[1,2]

[1]Department of Hematology, Zhongnan Hospital of Wuhan University, Wuhan University, Wuhan, China; [2]Frontier Science Center for Immunology and Metabolism, Medical Research Institute, Wuhan University, Wuhan, China; [3]Department of Hematology, The Affiliated Cancer Hospital of Zhengzhou University, Henan Cancer Hospital, Zhengzhou, China; [4]CAS Key Laboratory of Genomic and Precision Medicine, Beijing Institute of Genomics, Chinese Academy of Sciences and China National Center for Bioinformation, Beijing, China; [5]State Key Laboratory of Experimental Hematology, National Clinical Research Center for Blood Diseases, Institute of Hematology and Blood Diseases Hospital, Chinese Academy of Medical Sciences and Peking Union Medical College, Tianjin, China; [6]Department of Biomolecular Medicine, Ghent University, Ghent, Belgium; [7]Bio-Med Big Data Center, the First Affiliated Hospital, Zhejiang University School of Medicine, Hangzhou, China and [8]Department of Diagnostic Sciences, Ghent University, Ghent, Belgium

**HG, JX and PX contributed equally as first authors.*

Correspondence: H. Liu
hudanliu@whu.edu.cn

P. Van Vlierberghe
pieter.vanvlierberghe@ugent.be

Received: September 7, 2022.
Accepted: February 22, 2023.
Early view: March 2, 2023.

https://doi.org/10.3324/haematol.2022.282066

Abstract

RNA-binding proteins (RBP) have emerged as essential regulators that control gene expression and modulate multiple cancer traits. T-cell acute lymphoblastic leukemia (T-ALL) is an aggressive hematologic malignancy derived from transformation of T-cell progenitors that normally undergo discrete steps of differentiation in the thymus. The implications of essential RBP during T-cell neoplastic transformation remain largely unclear. Systematic evaluation of RBP identifies RNA helicase DHX15, which facilitates the disassembly of the spliceosome and release of lariat introns, as a T-ALL dependency factor. Functional analysis using multiple murine T-ALL models demonstrates the essential importance of DHX15 in tumor cell survival and leukemogenesis. Moreover, single-cell transcriptomics reveals that *DHX15* depletion in T-cell progenitors hinders burst proliferation during the transition from double-negative to double-positive cells ($CD4^-CD8^-$ to $CD4^+CD8^+$). Mechanistically, abrogation of DHX15 perturbs RNA splicing and leads to diminished levels of *SLC7A6* and *SLC38A5* transcripts due to intron retention, thereby suppressing glutamine import and mTORC1 activity. We further propose a DHX15 signature modulator drug ciclopirox and demonstrate that it has prominent anti-T-ALL efficacy. Collectively, our data highlight the functional contribution of DHX15 to leukemogenesis through regulation of established oncogenic pathways. These findings also suggest a promising therapeutic approach, i.e., splicing perturbation by targeting spliceosome disassembly, may achieve considerable anti-tumor efficacy.

Introduction

Normal T-cell development is a strictly regulated process in which hematopoietic progenitor cells migrate from the bone marrow to the thymus and differentiate from early T-cell progenitors into mature T cells.[1] During this maturation process, accumulation of multiple oncogenic lesions can drive immature thymocytes into uncontrolled clonal expansion and cause T-cell acute lymphoblastic leukemia (T-ALL),[2] which accounts for 10-15% of pediatric and 20-25% of adult cases of ALL.[3] Although the use of intensified cytotoxic drugs significantly improves the clinical prognosis in pediatric patients, the outcomes of adult patients remain poor.[4] More than 50% of adult patients with T-ALL do not achieve a complete remission or relapse after consolidated chemotherapy, highlighting the need for improved therapeutic interventions.[5]

A large body of data indicates that abnormal RNA-binding protein (RBP) expression/activity is a driving force of leukemia progression and an attribute of aggressive forms of disease.[6] Frequent somatic mutations in RBP that serve as splicing factors have been found in patients with mye-

loid leukemia, resulting in pathologically altered splicing which promotes the initiation and/or maintenance of leukemia.[7] Targeting strategies against crucial splicing factors represents an excellent therapeutic opportunity to improve outcomes of leukemia treatments.[8] However, such mutations have not yet been found in T-ALL, and the RBP dependency in T-ALL remains to be understood.

DEAH-box helicase 15 (*DHX15*) encodes an outstanding member of the DEAD/H-box RNA helicase family, characterized by the conserved DEAH (Asp-Glu-Ala-His) motif in the helicase domain.[9] According to early studies on its yeast ortholog Prp43, DHX15 has cellular functions in the last step of splicing by facilitating the release of lariat introns and disassembly of the spliceosome.[10-12] Cryo-electron microscopy structure analysis has shown that DHX15 is a key subunit in the intron lariat spliceosome complex in both yeast and humans, providing mechanistic insight into how DHX15 engages in spliceosome disassembly.[13,14] Accumulating evidence suggests a prominent role for DHX15 in human cancers,[15,16] although whether and how aberrant DHX15 expression leads to deregulated RNA splicing and contributes to tumorigenesis remains largely unclear.

We here identify DHX15, transcriptionally activated by oncogenic MYB, as a dependency factor in the pathogenesis of T-ALL. Intriguingly, specific ablation of *Dhx15* in the T-cell lineage resulted in a blockade of burst proliferation during the transition from the double-negative (DN) to double-positive (DP) stage, from which T-ALL arises. DHX15 is therefore a crucial RBP during T-cell development, which is hijacked by transformed T cells to confer neoplastic phenotypes. Mechanistically, aberrant expression of DHX15 leads to cancer-specific mis-spliced events associated with mTORC1 activation. Our data thus highlight the importance of the MYB-DHX15-mTORC1 axis in T-cell leukemogenesis, and the possibility of targeting DHX15 for therapeutic purposes.

Methods

Cell cultures

Human T-ALL cell lines KOPTK1, CUTLL1 and MOLT-3 were kindly provided by Dr Warren Pear (University of Pennsylvania). 293T, CCRF-CEM and Jurkat cell lines were purchased from American Type Culture Collection (ATCC). Human primary specimens were obtained with informed consent from Zhongnan Hospital of Wuhan University. Cell culture details are provided in the *Online Supplementary Material*.

Mice

Dhx15$^{fl/fl}$ mice were obtained from Biocytogen. *Lck*-Cre mice (JAX: 003802) and *Mx1*-Cre mice (JAX: 003556) were kindly provided by Dr Jinyong Wang and Dr Haojian Zhang, respectively. NOD.Cg-Prkdcscid Il2rgtm1Vst/Vst (NPG) mice were from Vitalstar. All animal experiments were performed under animal ethical regulations and the study protocol was approved by the Institutional Animal Care and Use Committee of Wuhan University.

NOTCH1-induced T-cell acute lymphoblastic leukemia mouse model

The NOTCH1-induced T-ALL model was established as previously decribed.[17] Briefly, bone marrow cells were isolated from 8-week-old donor mice. Lineage negative (Lin$^-$) cells were enriched using a Lineage Cell Depletion Kit (Miltenyi Biotec), and pre-stimulated for 24 h in Dulbecco modified Eagle medium (Gibco) containing 20% fetal bovine serum (Gibco), 1% penicillin/streptomycin (Hyclone), 20 ng/mL murine FLT3-L, 20 ng/mL murine thrombopoietin and 100 ng/mL murine stem cell factor (PeproTech). Cells were then transduced with MigR1-ICN1 retroviruses and centrifuged in the presence of 6 μg/mL polybrene. A second round of transduction was carried out on the next day. One million cells were then transplanted into sub-lethally (5.5 Gy) irradiated 8-week-old C57BL/6 female mice by tail vein injection.

High-throughput sequencing

For single-cell RNA sequencing, single cells were captured in droplet emulsions using a GemCode Single-Cell Instrument (10xGenomics). Libraries were constructed using Chromium Single-Cell 3′ Library and Gel Bead Kit V3.1 (10xGenomics), and sequenced using Illumina NovaSeq 6000. We demultiplexed the sequencing reads into single cells according to unique barcode sequences and aligned them to the mm10 reference using Cell Ranger (version 6.0.2). We merged the single-cell expression data from *Dhx15*$^{fl/fl}$ and *Dhx15* knockout (KO) thymocytes and eliminated potential doublets using Scanpy (version 1.7.1).[18] Uniform manifold approximation and projection was used to visualize the distribution of cells in the projection of the significant principal components and cells were clustered using the Leiden algorithm.[19] Trajectory analysis was performed using Monocle 3. Cell cycle states (G1, S, G2/M) were annotated by scoring gene sets with Scanpy. Details on bulk RNA sequencing and RNA immunoprecipitation sequencing (RIP-Seq) are provided in the *Online Supplementary Material*.

Statistical analysis

Data were analyzed using GraphPad Prism 8. Statistical significance was calculated by unpaired *t* tests between two groups or by one-way analysis of variance for multiple groups. Log-rank analysis was used to evaluate differences in Kaplan-Meier survival curves. Differences were considered statistically significant when $P<0.05$.

Results

Aberrant expression of RNA helicase DHX15 in human T-cell acute lymphoblastic leukemia

We compared the expression profiles between 21 normal thymocyte and 57 T-ALL samples,[20] and revealed metabolism of RNA as the most significant enriched term across all differentially expressed genes (Figure 1A, B). Since RBP are key players in RNA metabolism, we then focused on analyzing the expression of 490 well-defined RBPs containing canonical RNA-binding motifs[21,22] in two pairs of independent datasets of normal thymocyte and T-ALL samples[20,23,24] and searched for upregulated RBP in leukemia. There were eight overlapping genes commonly elevated in T-ALL with a false discovery rate less than 0.01 (Figure 1C, *Online Supplementary Figure S1A*). Based on results from a previously performed CRISPR-Cas9 screen of RBP in Jurkat cells,[22] we identified DHX15 as the most highly dependent factor among the eight candidates (Figure 1C). Gene expression studies, based on multiple human leukemia datasets,[20,23-26] verified that *DHX15* expression was significantly higher in T-ALL patient samples than in normal thymocytes or bone marrow cells (Figure 1D, *Online Supplementary Figure S1B*). We further confirmed that *DHX15* mRNA and protein were more abundant in seven human T-ALL cell lines relative to normal human thymocytes (Figure 1E, F). Consistently, elevated DHX15 protein expression was also observed in primary human T-ALL cells (Figure 1F, *Online Supplementary Table S2*). Of note, increased *DHX15* expression was not associated with either specific T-ALL subgroups or *NOTCH1* mutational status (*Online Supplementary Figure S1C, D*). We next analyzed the Cancer Cell Line Encyclopedia[27] and found the highest expression of *DHX15* in T-ALL among human cancer cell lines from 38 tumor types (*Online Supplementary Figure S1E*). Taken together, these data demonstrate a global increase of *DHX15* expression in T-ALL.

MYB directly activates *DHX15* transcription in T-cell acute lymphoblastic leukemia

To understand the molecular mechanism underlying *DHX15* upregulation in T-ALL, we tested the dependency of DHX15 expression on a panel of prominent transcription factors previously identified in T-ALL. Notably, only short hairpin RNA (shRNA)-mediated *MYB* knockdown significantly reduced DHX15 expression at mRNA and protein levels (Figure 2A, B, *Online Supplementary Figure S2*). Levels of cleaved caspase-3 were comparable in these samples, ruling out nonspecific DHX15 loss due to cell death upon *MYB* knockdown (Figure 2B). We analyzed previously reported chromatin immunoprecipitation sequencing data and found a strong binding signal of MYB in the *DHX15* locus,[28] along with histone H3 lysine 27 acetylation (H3K27ac), a marker of active transcription (Figure 2C). We next performed conventional chromatin immunoprecipitation assays and validated a significant increase in MYB recruitment to the DHX15 promoter region (Figure 2D). We revealed three putative MYB responsive elements (YAACG/TG)[29] proximal to the transcription start site (-436 bp, +137 bp, +143 bp) and constructed the promoter sequence in a luciferase reporter vector. The *DHX15* reporter was strongly activated by enforced MYB expression whereas the reporter with mutant MYB binding sites was barely induced (Figure 2E). Furthermore, gene expression profiling of 562 primary T-ALL samples[30-33] revealed a significant correlation between *DHX15* and *MYB* mRNA levels ($R=0.55$, $P<2.2\times10^{-16}$) (Figure 2F). Collectively, this evidence demonstrates that oncogenic MYB specifically binds to *DHX15* for direct transcriptional activation in T-ALL.

Essential role of DHX15 in sustaining T-cell acute lymphoblastic leukemia cell survival in vitro and in vivo

We next determined the role of DHX15 in T-ALL cell growth and survival using two shRNA. Both shRNA markedly depleted *DHX15* expression at the mRNA and protein levels in human T-ALL KOPTK1 and CUTLL1 cells (Figure 3A), resulting in substantial growth inhibition (Figure 3B) and robust apoptosis (*Online Supplementary Figure S3A, B*). Cell cycle analysis showed a decreased G2/M and an increased sub-G1 phase distribution in cells devoid of *DHX15* expression (*Online Supplementary Figure S3C*). To rule out the possibility of an off-target effect of shRNA, we reconstituted *DHX15* expression by ectopically expressing its coding region resistant to shRNA targeting the 3′ untranslated region (sh1) (*Online Supplementary Figure S3D*). Exogenous DHX15 rescued cell growth and viability to a great extent (*Online Supplementary Figure S3E*). Notably, while T-ALL cells showed a strict dependency on DHX15 expression, DHX15 loss led to relatively mild growth defects in normal $CD34^+$ hematopoietic stem and progenitor cells (HSPC) (*Online Supplementary Figure S3F-H*).

To examine the *in vivo* significance of DHX15 in T-ALL, we established human xenografts using MOLT-3 cells co-expressing green fluorescent protein (GFP) as a surrogate marker and firefly luciferase to visualize leukemia cell expansion *in vivo*. Control or *DHX15*-depleted MOLT-3 cells were intravenously injected into NPG mice (*Online Supplementary Figure S4A, B*). As shown in Figure 3C and *Online Supplementary Figure S4C*, we observed a marked delay in leukemia progression in mice receiving *DHX15*-deficient cells, as determined by bioluminescent imaging. When control mice became moribund and exhibited severe splenomegaly, mice bearing *DHX15*-depleted cells showed spleens of normal size (Figure 3D). Moreover, flow cytometry analysis of spleen and bone marrow cells from xenografted mice revealed much lower percentages of GFP^+ infiltrating leukemia

cells with *DHX15* depletion (Figure 3E), which correlated with significantly prolonged survival (Figure 3F). These observations support the indispensable role of DHX15 in T-ALL progression *in vivo*.

DHX15 depletion inhibits NOTCH1-driven T-cell leukemogenesis

We then assessed the requirement of *DHX15* in T-ALL initiation, and generated a conditional *Dhx15* KO mouse

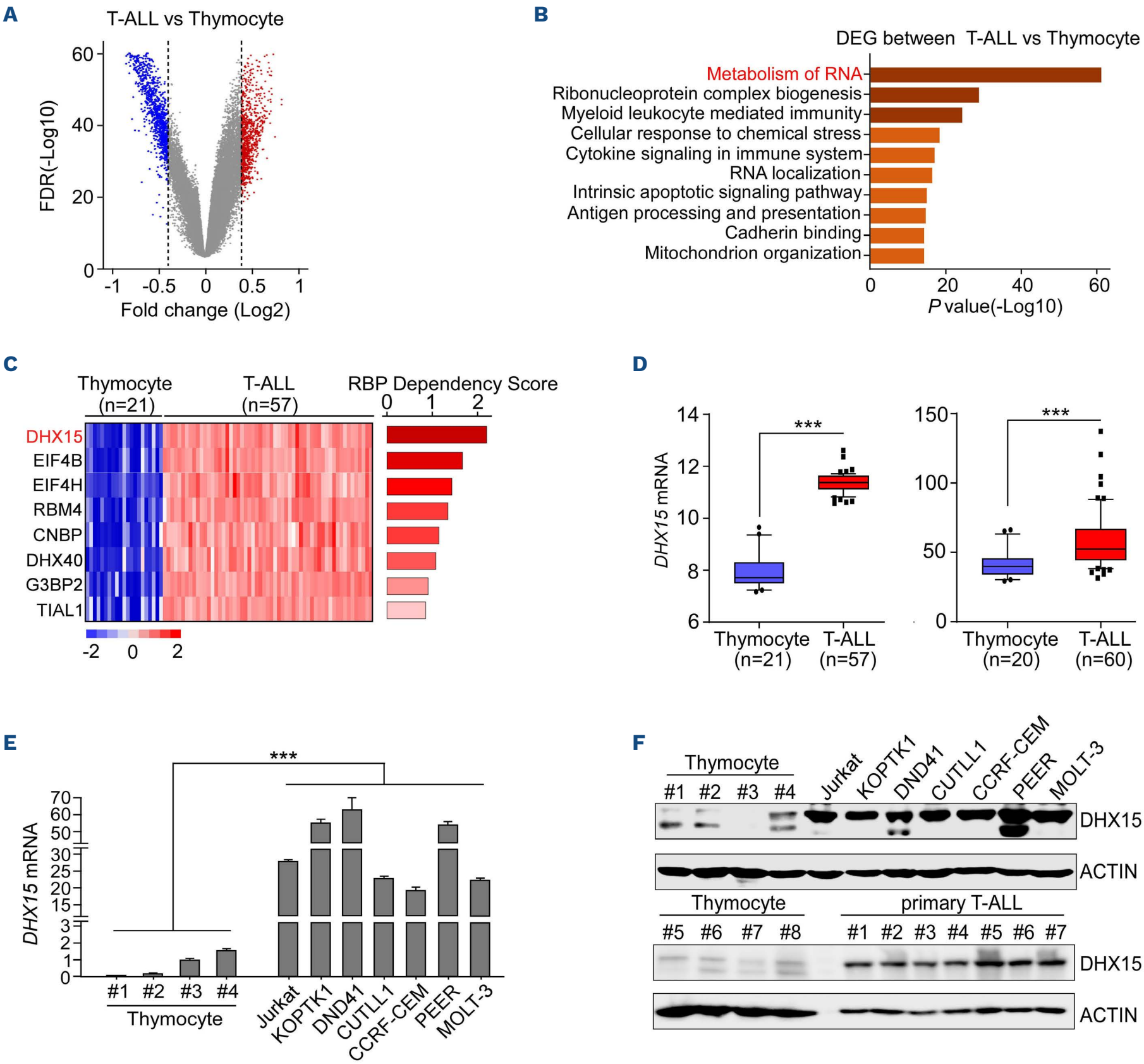

Figure 1. Elevated *DHX15* expression in T-cell acute lymphoblastic leukemia. (A) Volcano plots showing the differentially expressed genes (fold change >1.3, false discovery rate <0.01) between T-cell acute lymphoblastic leukemia (T-ALL) patients' samples (N=57, GSE33469) and normal thymocyte samples (n=21, GSE33470). (B) Bar graph showing enriched gene ontology terms across differentially expressed genes in (A). (C) Heatmap presentation of eight commonly elevated RNA-binding proteins (RBP) in 57 T-ALL patients' samples (GSE33469) as compared to 21 normal thymocyte samples (GSE33470) from dataset 1 (left). Bar plots showing dependency scores of the eight genes from the RBP CRISPR-Cas9 screen in Jurkat cells (right).[22] (D) *DHX15* mRNA expression presented in dataset 1 (left) and dataset 2 (60 T-ALL patients' samples and 20 normal thymocyte samples from GSE110637 and GSE151081) (right). The distributions of *DHX15* mRNA expression are presented in box-and-whisker plots with the median value (line). Boxes and whiskers depict 25-75 and 10-90 percentiles respectively. Values outside of this range are plotted as individual points. ***P<0.001. (E) Analysis of *DHX15* mRNA in normal human thymocytes and T-ALL cell lines by quantitative polymerase chain reaction. Data shown represent the means (± standard deviation), ***P<0.001. (F) Immunoblots of DHX15 in normal human thymocytes, T-ALL cell lines (upper) and primary patients' T-ALL cells (bottom), as indicated. ACTIN served as a loading control. FDR: false discovery rate; DEG: differentially expressed genes

strain that allows specific depletion of *Dhx15* starting at the DN2-3 stage of thymocyte development. This was obtained by crossing *Dhx15*$^{fl/fl}$ mice that carry LoxP sites flanking the coding exon 2 of the *Dhx15* gene with mice expressing Cre under the control of the proximal *Lck* promoter (*Lck*-Cre) (*Online Supplementary Figure S5A*). Deletion of exon 2 of the *Dhx15* gene results in a premature stop codon and truncated RNA is subject to nonsense mediated decay (*Online Supplementary Figure S5A*). We purified CD4$^-$CD8$^-$ double-negative (DN2-3 and DN4) and

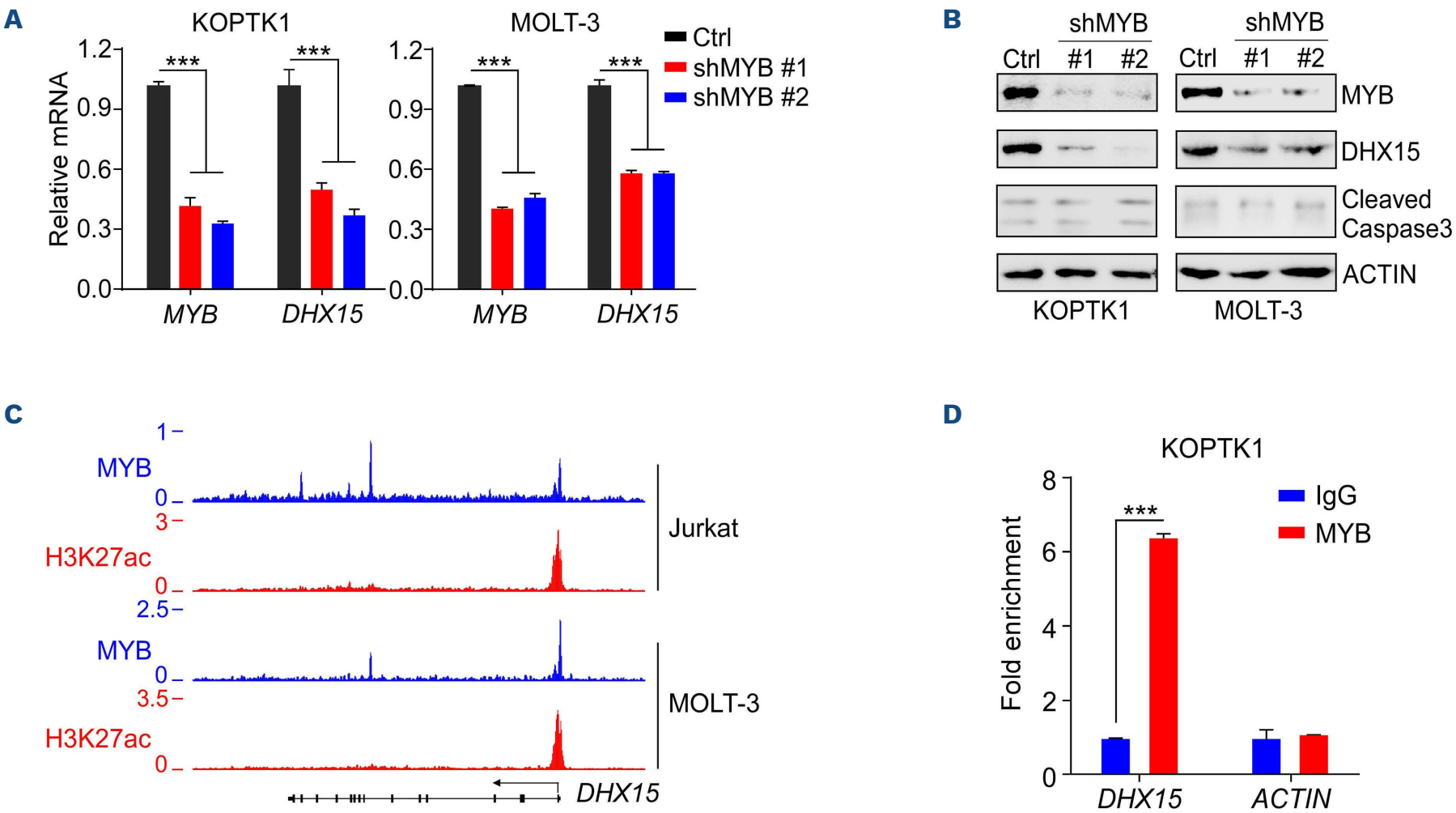

Figure 2. *DHX15* is a direct MYB transcriptional target. (A, B) KOPTK1 and MOLT-3 cells were transduced with lentiviruses expressing short hairpin (sh)RNA targeting control (Ctrl) or *MYB* (#1, #2). *MYB* and *DHX15* mRNA were analyzed by quantitative polymerase chain reaction. (B) Immunoblots of MYB, DHX15 and cleaved caspase-3 in KOPTK1 and MOLT-3 cells after MYB knockdown. ACTIN served as a loading control. (C) Chromatin immunoprecipitation (ChIP) sequencing data of MYB and H3K27ac in Jurkat and MOLT-3 cells (GSE59657) show binding signals proximal to the *DHX15* locus. (D) Binding of MYB to the *DHX15* or *ACTIN* promoter (negative control) was analyzed by ChIP in CUTLL1 cells. Averages of fold enrichment between MYB and isotype IgG are shown. (E) Schematic presentation of MYB binding sites (-436 bp, +137 bp, +143 bp) on the *DHX15* promoter. The potential MYB responsive elements (RE-WT) and the mutants (Mut) are shown as indicated (left). Luciferase reporter activities of the *DHX15* promoter containing MYB RE-WT, including RE1-3, or RE-Mut were detected in the presence of ectopically expressed MYB in 293T cells. Reporter activities relative to empty pGL3-Basic vector (Vector) are shown (right). (F) Scatter plot showing the co-expression pattern of *DHX15* and *MYB* in 562 T-acute lymphoblastic leukemia samples from databases of Genotypes and Phenotypes (dbGaP) (phs000218), European Genome Phenome archive (EGAS00001004700), National Genomics Data Center (HRA000122 and HRA000113) and Japanese Genotype-phenotype Archive (JGAS000090). Data shown in (A), (D) and (E) represent the means (± standard deviation), ***P<0.001.

CD4⁺CD8⁺ double-positive (DP) thymocytes from the *Lck*-Cre *Dhx15*$^{fl/fl}$ strain (hereafter termed *Dhx15* KO) and confirmed the knockout efficiency in these subsets (*Online Supplementary Figure S5B, C*).

To generate the T-ALL mouse model, lineage negative (Lin⁻) bone marrow cells from either *Dhx15*$^{fl/fl}$ or *Dhx15* KO mice were isolated and transduced with the MSCV-IRES-GFP retroviral vector expressing intracellular NOTCH1

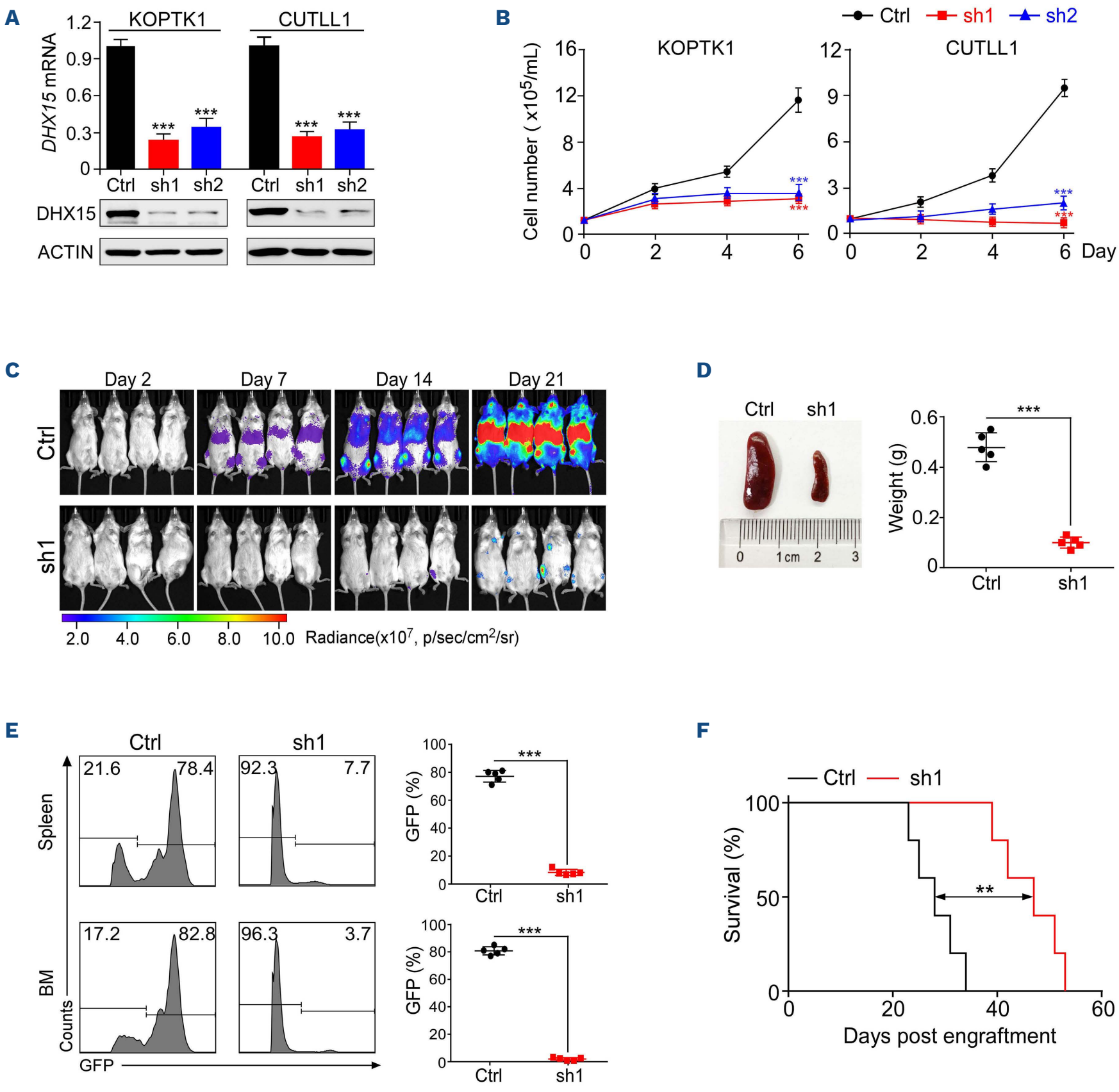

Figure 3. DHX15 is required to maintain T-cell acute lymphoblastic leukemia cell survival *in vitro* and *in vivo*. (A) KOPTK1 and CUTLL1 cells were transduced with lentiviruses expressing short hairpin (sh)RNA targeting control (Ctrl) or *DHX15* (sh1: targeting 3′UTR and sh2: targeting coding region). *DHX15* mRNA and protein were analyzed by quantitative polymerase chain reaction (top) and immunoblot (bottom). (B) Live KOPTK1 and CUTLL1 cells were counted at the indicated time points and cell growth was plotted as shown. (C) Human T-cell acute lymphoblastic leukemia MOLT-3 cells, expressing both luciferase and green fluorescence protein (GFP) markers, were infected with shRNA targeting *DHX15* mRNA (sh1) or control. Two million GFP⁺ cells were injected into irradiated NPG mice, followed by *in vivo* bioimaging to assess leukemia progression. Representative images of leukemia burden assessed by bioimaging in xenografted mice. Time points after engraftment are shown on the top. (D) Representative spleen images are shown (left) with spleen weights plotted (right) at the 28th day after transplantation. (E) Representative flow cytometry images of GFP⁺ spleen and bone marrow cells from mice shown in (D) (left). GFP⁺ percentages were plotted and are shown on the right (N=5 per group). (F) Kaplan-Meier survival curves of MOLT-3 xenografts (N=5 per group). ***P*<0.01; ****P*<0.001. BM: bone marrow.

(ICN1), then transplanted into irradiated recipient mice (Figure 4A). Mice transplanted with ICN1-expressing *Dhx15*$^{fl/fl}$ cells showed an early increase in the frequency of GFP$^+$ leukemia cells in peripheral blood which developed into overt CD4$^+$CD8$^+$ T-ALL within 6 weeks (Figure 4B, C, *Online Supplementary Figure S5D*), concomitant with accumulation of lymphoblasts in the peripheral blood (Figure 4D). In contrast, mice transplanted with *Dhx15* KO progenitors showed a marginal increase of lymphoblastic leukemia cells over time (Figure 4B-D). Whereas all the mice transplanted with *Dhx15*$^{fl/fl}$ cells developed severe splenomegaly from leukemic infiltration within 8 weeks, enlarged spleens were not detected in mice transplanted with *Dhx15* KO cells (Figure 4E). Histological examination of the spleens by hematoxylin-eosin and proliferating cell nuclear antigen staining confirmed much less leukemia infiltration as a result of *Dhx15* gene inactivation (Figure 4F). While all mice in the control cohort succumbed to T-ALL within 70 days, mice bearing *Dhx15* KO cells exhibited significantly prolonged survival (Figure 4G). Of note, almost half of the mice transplanted with *Dhx15* KO cells were viable and remained disease-free over 12 months after transplantation (Figure 4G), suggesting that inactivation of *Dhx15* significantly suppresses leukemia onset and reduces the penetrance of ICN1-induced T-ALL. We hardly detected Dhx15 protein expression in leukemia cells derived from *Dhx15* KO donors (*Online Supplementary Figure S5E*), indicating that these cells were not escapers from the Cre-induced inactivation and that other mechanisms may be involved in leukemogenesis despite *Dhx15* KO. Moreover, knockout of *Dhx15* barely affected HSPC infiltration into the bone marrow and spleen at the early stage (*Online Supplementary Figure S5F, G*), ruling out the possibility that the phenotype of delayed leukemogenesis was due to defective homing or engraftment of HSPC. These findings underscore the essential importance of DHX15 in T-ALL initiation.

To test the effect of *Dhx15* deletion on T-ALL maintenance, we also generated *Mx1*-Cre *Dhx15*$^{fl/fl}$ mice for the NOTCH1-induced T-ALL model, which allows inducible *Dhx15* KO following pIpC (poly I:C) treatment (*Online Supplementary Figure S6A, B*). As shown in *Online Supplementary Figure S6C, D*, pIpC injection significantly impaired GFP$^+$ leukemia cell expansion in peripheral blood, bone marrow and spleen. Taken together, these data support the notion that DHX15 is required for both T-ALL initiation and maintenance.

DHX15 is required for normal T-cell development

Anatomical analysis of *Dhx15* KO mice revealed a striking reduction in thymus size and cellularity (Figure 5A, *Online Supplementary Figure S7A*), which was much more pronounced in homozygotes than in heterozygotes (*Online Supplementary Figure S7B*), without a perceptible abnormality in spleen size (*Online Supplementary Figure S7C*). Immunohistological staining of Ki67 and cleaved caspase 3 demonstrated that decreased thymic cellularity in *Dhx15* KO mice resulted mainly from impaired cell proliferation but not enhanced cell death (*Online Supplementary Figure S7D*). As an expected outcome, mature CD3$^+$, CD4$^+$ and CD8$^+$ T cells declined dramatically in the peripheral blood and spleen of *Dhx15* KO animals (*Online Supplementary Figure S7E, F*).

We attempted to determine at which developmental stage *Dhx15* has a major impact. Flow cytometry analysis of CD4 and CD8 expression revealed substantial reductions in the proportion and cellularity of DP thymocytes in *Dhx15* KO mice, concomitant with accumulation of DN progenitors (Figure 5B, *Online Supplementary Figure S7G*). We further investigated the DN populations and observed increased DN3-4 cells in *Dhx15* KO mice compared to those in *Dhx15*$^{fl/fl}$ controls (*Online Supplementary Figure S7H*). Again, the altered cellularity was not associated with enhanced apoptotic cell death (*Online Supplementary Figure S7I*).

To further clarify the heterogeneity of thymocyte subsets and the abnormal gene expression profiles in the absence of *Dhx15*, we performed single-cell RNA sequencing using the 10x Genomics platform on isolated single cells from thymus with or without *Dhx15* expression (*Online Supplementary Figure S8A*). A total of 9,434 and 8,484 live cells were obtained from *Dhx15*$^{fl/fl}$ and *Dhx15* KO thymus, respectively. Cells were clustered into nine annotated T-cell subgroups based on previously reported marker gene expression (*Online Supplementary Figure S8B, C*):[34,35] DN cells, DN-to-DP transitional cells (DN/DPtrans), DP cells undergoing rearrangement (DPre1-4), DP cells under selection (DPsel1-2), and CD4/CD8 single-positive (SP) cells (Figure 5C). Consistent with flow cytometry analysis, cell type composition and pseudotime analysis showed substantial reductions of DP and SP populations, and accumulation of DN progenitors in *Dhx15* KO thymus (Figure 5D, *Online Supplementary Figure S8D*). We next compared the gene expression profile of each cluster between two groups, and found the most striking differential expression in the DN-to-DP transitional cluster (*Online Supplementary Figure S8E*). Gene ontology analysis revealed that the majority of downregulated genes in *Dhx15* KO cells were involved in cell cycle (Figure 5E). Cell cycle distribution and scoring analysis validated a significant impaired G2/M phase in *Dhx15* KO cells (Figure 5F), consistent with the proliferation defect upon *Dhx15* inactivation. Taken together, these results demonstrate that DHX15 is a key regulator of progenitor T-cell proliferation.

DHX15 loss alters RNA splicing and impairs mTORC1 activation

We next sought to understand the mechanism underlying the phenotypic consequences resulting from *DHX15* de-

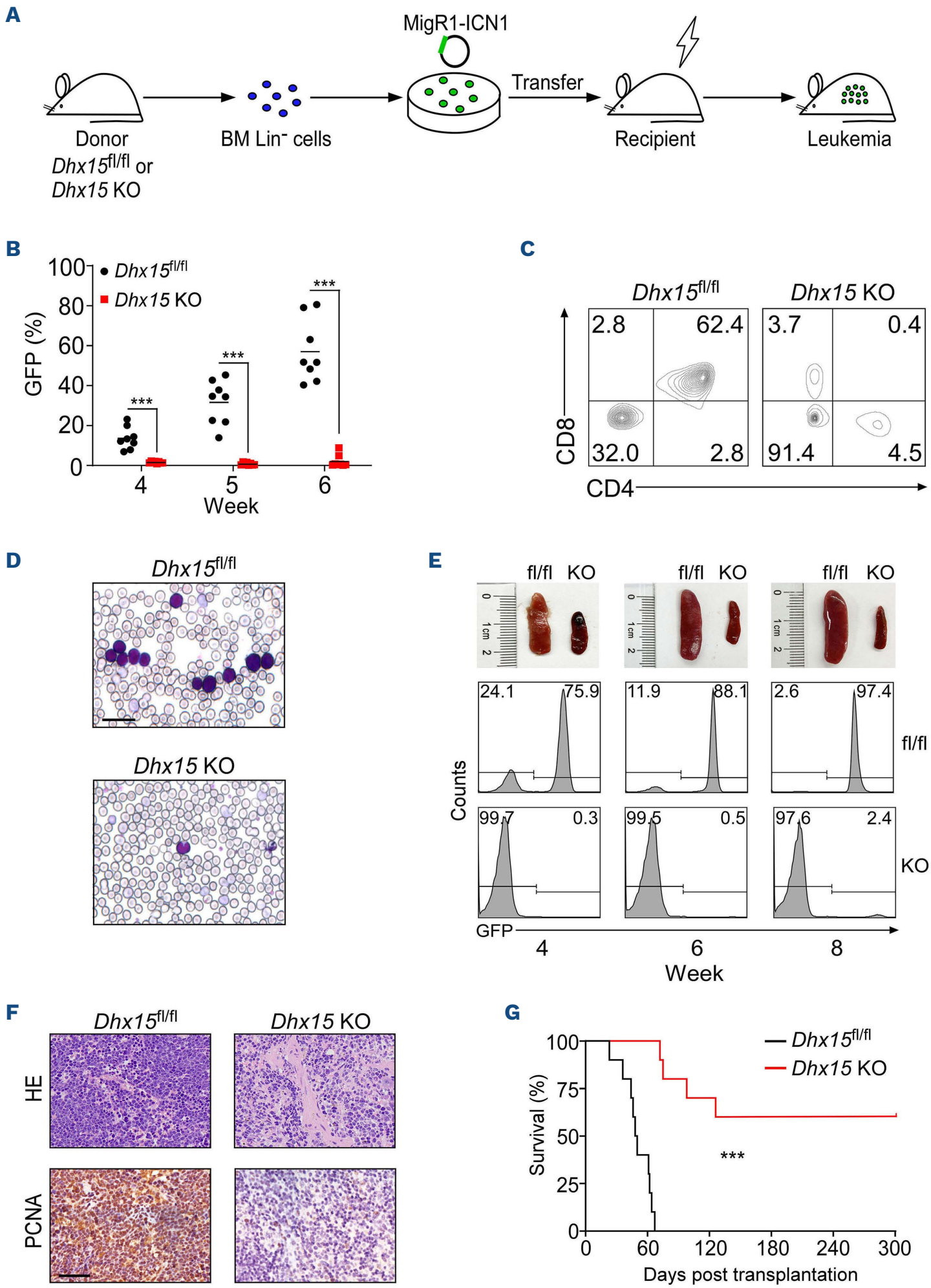

Figure 4. *DHX15* deficiency impedes T-cell leukemogenesis *in vivo*. (A) Graphical illustration of the mouse model of NOTCH1-induced T-cell acute lymphoblastic leukemia. Lin⁻ bone marrow cells from *Dhx15*$^{fl/fl}$ or *Dhx15* knockout (KO) mice were transduced with MigR1-ICN1 retroviruses and transplanted into irradiated recipient mice, followed by assessment of leukemia dissemination. (B) Percentages of green fluorescent protein (GFP)⁺ cells in peripheral blood at the indicated times after transplantation (N=8 per group). (C) Representative flow cytometry analysis of CD4⁺CD8⁺ double-positive leukemia cells 6 weeks after transplantation. (D) Representative peripheral blood smear examined by Wright-Giemsa staining. Scale bar, 25 μm. (E) Spleen images (top) and flow cytometry analysis of GFP⁺ leukemia cells (bottom) at the indicated times after transplantation. (F) Representative images of spleen histology stained with hematoxylin and eosin (top) and immunohistochemical staining of proliferating cell nuclear antigen (bottom). Scale bar, 50 μm. (G) Kaplan-Meier survival curves for recipients of ICN1-transduced Lin⁻ bone marrow cells from *Dhx15*$^{fl/fl}$ or *Dhx15* KO donor mice (N=10 per group). ***P<0.001. BM: bone marrow; HE: hematoxylin and eosin; PCNA: proliferating cell nuclear antigen.

pletion. DHX15 has been reported to regulate RNA splicing by recycling spliceosomes, modulating 5'/3' splice site selection,[9] and mediating RNA missplicing.[36] To identify key downstream effectors modulated by DHX15, we evaluated splicing changes by RNA sequencing in CUTLL1 cells with or without *DHX15* expression. "Percentage spliced in" values were used to quantify five alternative splicing events upon *DHX15* loss, including skipped exons, mutually exclusive exons, alternative 5' splice sites, alternative 3' splice sites, and retained introns. We detected widespread splicing changes in *DHX15*-depleted cells with skipped exons being the most frequently affected alternative splicing event. We also observed a distinct transcriptomic landscape which may result from altered RNA splicing (Figure 6A, *Online Supplementary Figure S9A*). By overlapping the targets undergoing differential splicing and expression from two independent shRNA we were able to identify 466 DHX15-responsive genes whose expression changes were con-

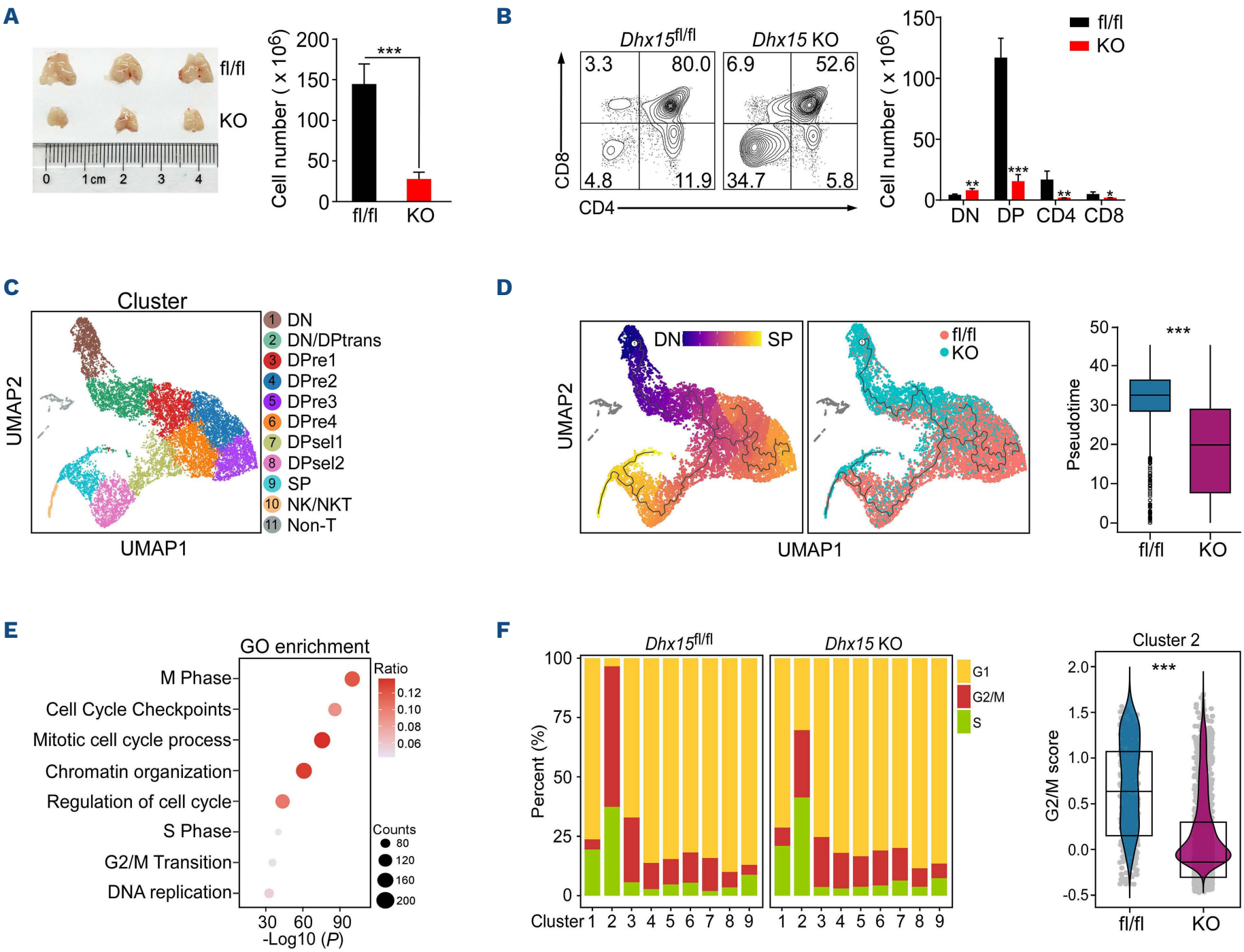

Figure 5. *DHX15* deficiency hampers thymocyte development. (A) Thymus morphology (left) and cellularity (right) of 6-week-old *Dhx15*$^{fl/fl}$ and *Dhx15* knockout (KO) mice (N=5 per group). (B) Representative flow cytometry analysis of CD4$^+$ and/or CD8$^+$ thymocytes. Cellularity in absolute numbers is shown on the right (N=5 per group). (C) Uniform manifold approximation and projection (UMAP) visualization of the cellular composition of *Dhx15*$^{fl/fl}$ and *Dhx15* KO thymi colored by cell type as indicated. (D) Pseudotime cell trajectories from the double-negative to single-poisitive stage predicted by Monocle 3 and visualized by UMAP (left and middle). Box plot displaying pseudotime scores for *Dhx15*$^{fl/fl}$ and *Dhx15* KO thymocytes (right). (E) Bubble plot showing enriched gene ontology terms across downregulated genes of double-negative to double-positive transitional cells (Cluster 2 in C) in *Dhx15* KO thymocytes. (F) Bar graph showing cell cycle distribution of each cluster (Clusters 1-9 in C) from *Dhx15*$^{fl/fl}$ or *Dhx15* KO thymocytes (left). Violin plot showing the G2/M scores (calculated by Scanpy) for double-negative to double-positive transitional cells (Cluster 2 in C) in *Dhx15*$^{fl/fl}$ and *Dhx15* KO thymocytes (right). *P<0.05; **P<0.01; ***P<0.001. DN: double-negative (CD4$^-$CD8$^-$); DP: double-positive (CD4$^+$CD8$^+$); DN/DPtrans: DN-to-DP transition cells; DPpre1-4: DP cells undergoing rearrangement; DPsel1-2: DP cells under selection; SP: CD4/CD8 single-positive cells; NK/NKT: natural killer and natural killer T cells; Non-T: non-T cells; GO: gene ontology.

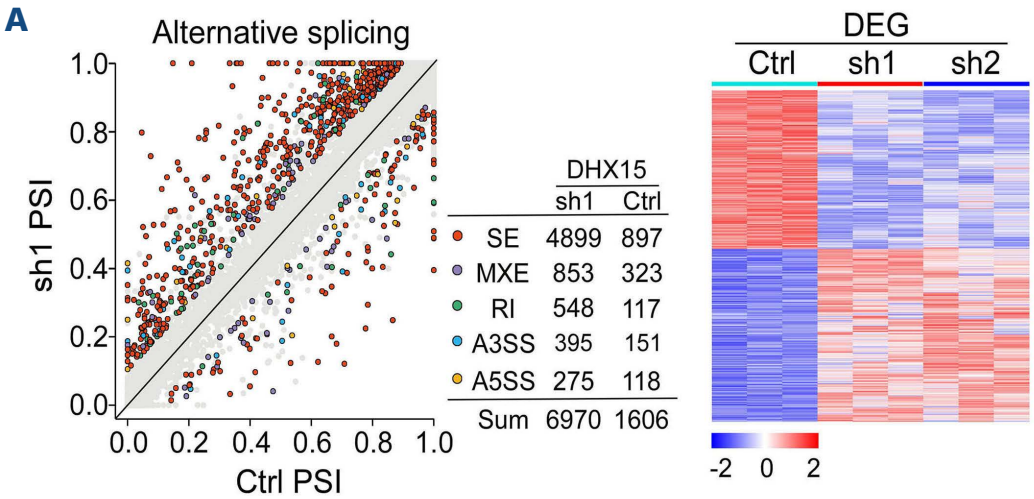

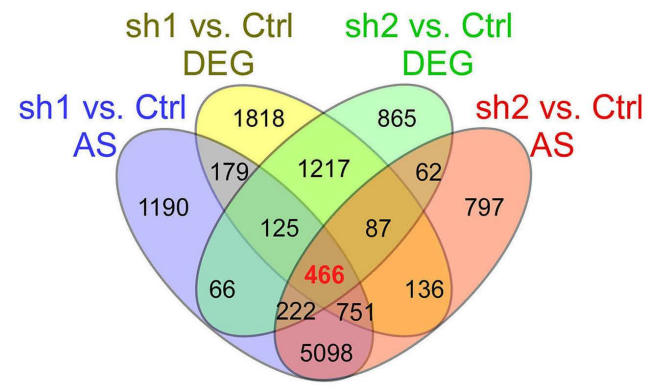

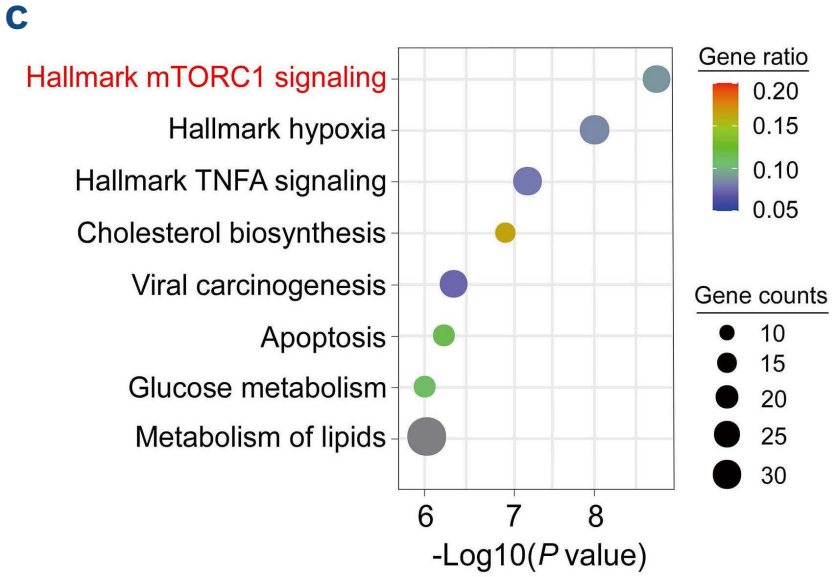

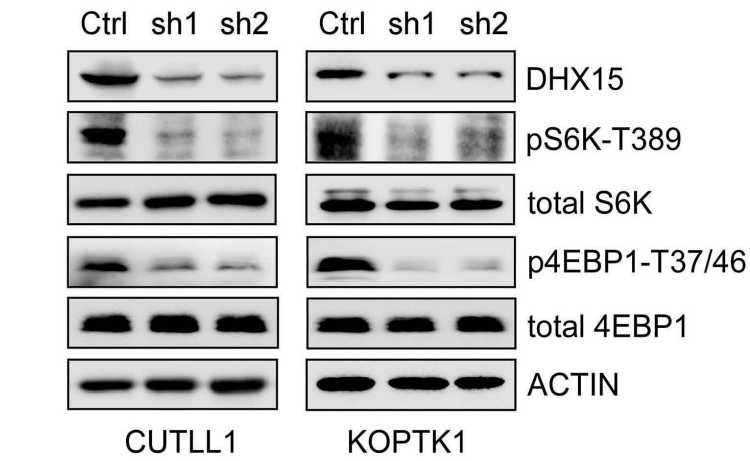

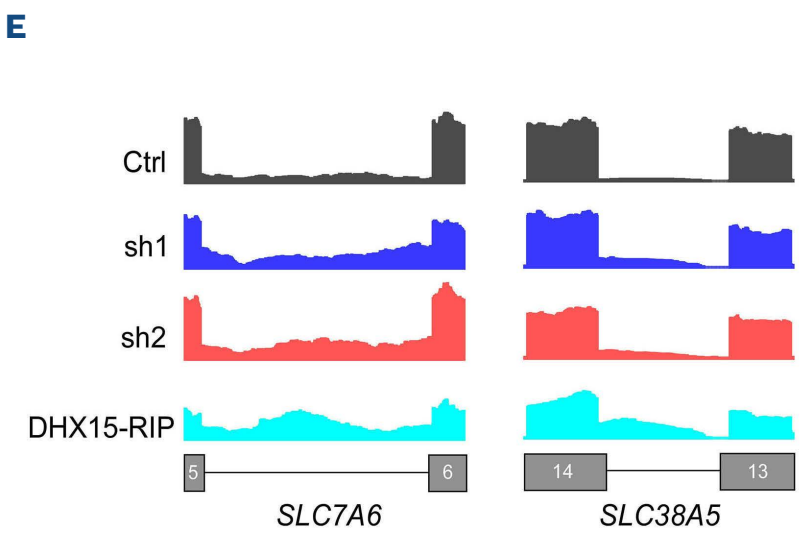

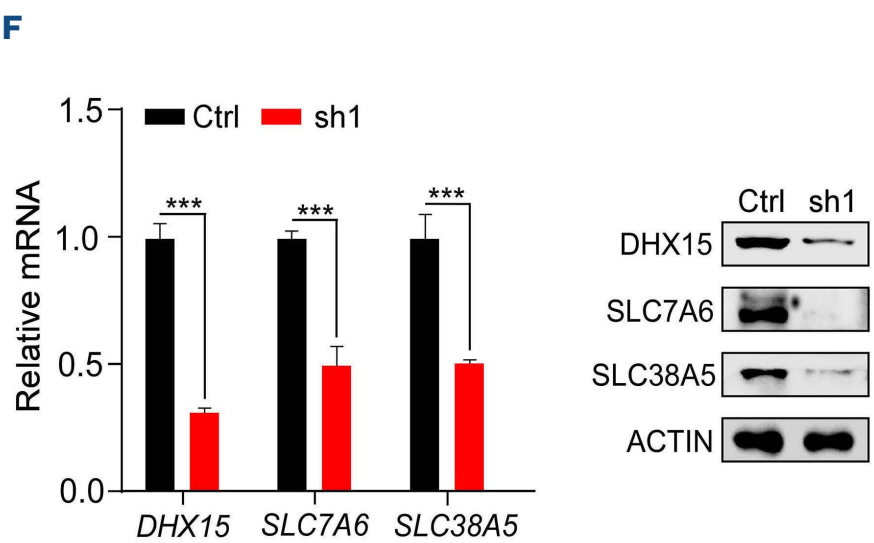

Figure 6. *DHX15* deficiency alters RNA splicing and leads to mTORC1 inactivation. (A) Scatterplot showing significant changes in alternative splicing (|ΔPSI|≥0.1) in CUTLL1 cells expressing DHX15 shRNA (sh1) or control (Ctrl). Counts of differentially spliced events in five types of alternative splicing are also shown (left). Heatmap showing differentially expressed genes (P<0.05) upon *DHX15* depletion (sh1 and sh2) in CUTLL1 cells (right). (B) Venn diagram showing the overlapping genes with alternative splicing and differential expression (P<0.05, fold change >1.5) in (A). (C) Bubble graph showing gene ontology enrichment of 466 overlapping genes (B) analyzed by Metascape (*www.metascape.org*); the enriched terms were illustrated and aligned by P values. (D) *DHX15* was depleted by shRNA (sh1 and sh2) in CUTLL1 and KOPTK1 cells. Phosphorylation of S6K (threonine 389) and 4EBP1 (threonine 37/46) was analyzed by immunoblot. (E) RNA-sequencing coverage plot of *SLC7A6* and *SLC38A5* in CUTLL1 cells with or without *DHX15* depletion, overlaid with anti-DHX15 RNA immunoprecipitation sequencing tracks. Gray bars represent indicated exons. (F) *DHX15* was depleted by shRNA (sh1) in CUTLL1 cells. *SLC7A6* and *SLC38A5* mRNA and protein were analyzed by quantitative polymerase chain reaction (left) and immunoblot (right). Data shown represent the means (± standard deviation), ***P<0.001. PSI: percentage splice in; SE: skipped exons; MXE: mutually exclusive exons; RI: retained introns; A3SS: alternative 3′ splice sites; A5SS: alternative 5′ splice sites; DEG: differentially expressed genes; AS: alternative splicing; RIP: RNA immunoprecipitation.

comitant with altered splicing (Figure 6B). Enrichment analysis of these genes revealed prominent downregulation of the mTORC1 pathway (Figure 6C), known to be required for cell cycle control[37] as well as T-ALL progression and T-cell development.[38] Moreover, gene set enrichment analysis (GSEA) showed the enrichment of mTORC1 signature genes in both CUTLL1 cells and DN/DP transitional cluster cells subjected to *DHX15* ablation (*Online Supplementary Figure S9B*). In support of this notion, *DHX15* deficiency significantly attenuated both S6K phosphorylation at threonine 389 and 4EBP1 phosphorylation at threonine 37/46, two classical markers of mTORC1 activation,[39] in CUTLL1 and KOPTK1 cells (Figure 6D), corroborating an essential role of DHX15 in sustaining mTORC1 activity.

Splicing analysis revealed retained introns in the mRNA encoding solute carrier family amino acid transporters SLC7A6 and SLC38A5, which import glutamine and activate mTORC1.[40,41] Furthermore, genome-wide DHX15-RNA interaction analyzed by RIP-Seq showed that DHX15 was capable of binding to these retained introns (Figure 6E), suggesting that efficient splicing of these genes is mediated by direct association of DHX15 to the mRNA transcripts. These intron-retained transcripts containing premature stop codons were subjected to nonsense mediated decay, leading to decreased mRNA and protein expression of SLC7A6 and SLC38A5 (Figure 6F, *Online Supplementary Figure S9C*). We also confirmed that knockdown of each transporter resulted in attenuation of mTORC1 signaling (*Online Supplementary Figure S9D*).

To verify that mTORC1 is a major downstream effector in response to DHX15 activity, we knocked down *TSC2*, the negative regulator of mTORC1 signaling,[42,43] and achieved constitutive activation in KOPTK1 cells. Sustained mTORC1 activation reversed the phenotype of massive cell death induced by *DHX15* ablation (*Online Supplementary Figure S9E*). Activation of mTORC1 by the small molecule agonist 3BDO[44] yielded the similar result of rescuing cell death (*Online Supplementary Figure S9F*). These studies demonstrate that the dependency of DHX15 in T-ALL is, at least in part, attributable to pathogenic splicing of genes involved in mTORC1 activation.

Identification of ciclopirox as a DHX15 modulator drug

Given the pro-leukemogenic role of DHX15 in multiple T-ALL models, we surmised that targeting DHX15 in leukemic lymphoblasts could be therapeutically beneficial. However, small molecules with DHX15 inhibitory potential are unavailable. We thus considered a drug repurposing strategy by interrogating the next-generation Connectivity Map, a large-scale compendium of gene expression readouts derived from tumor cells treated with bioactive small molecules.[45] We intended to search for compounds with gene expression signatures resembling that induced by *DHX15* depletion.

As shown in Figure 7A and *Online Supplementary Figure S10A*, this analysis identified ciclopirox, a broad-spectrum antifungal agent,[46] as a top hit as a *DHX15* inhibitory modulator. It is notable that this analysis also revealed rapamycin, the mTORC1 inhibitor, which mimics the effect induced by *DHX15* loss. Intriguingly, we observed profound *DHX15* loss in CUTLL1 and KOPTK1 cells treated with ciclopirox in a dose-dependent manner (Figure 7B, *Online Supplementary Figure S10B*). As mRNA and protein stability of DHX15 remained unaltered after ciclopirox exposure, it is most likely that ciclopirox downregulates DHX15 at the transcriptional level (*Online Supplementary Figure S10C*, *D*). We next compared the gene expression profiling of CUTLL1 cells treated with ciclopirox and cells subjected to *DHX15* depletion, and found a large number of overlapping genes that are clustered with analogous expression changes (Figure 7C, D). As further support, GSEA of differentially expressed genes upon ciclopirox treatment showed significant enrichment in the gene expression signature elicited by *DHX15* loss (Figure 7E). *Vice versa*, GSEA of differentially upregulated and downregulated genes upon *DHX15* depletion showed a highly significant enrichment in the gene expression signature responsive to ciclopirox exposure (*Online Supplementary Figure S10E*). Similar to *DHX15* ablation, administration of ciclopirox inhibited SLC38A5 and SLC7A6 expression as well as S6K and 4EBP1 phosphorylation (Figure 7F). These results argue for a convergent effect of ciclopirox treatment and *DHX15* deficiency in T-ALL. Following these findings, we next assessed the effects of ciclopirox treatment on a panel of human T-ALL cells as well as normal bone marrow cells. As shown in Figure 7G, administration of ciclopirox elicited a strong anti-leukemic effect on T-ALL cells, whereas it had a minimal effect on normal bone marrow cells. More importantly, enforced DHX15 expression significantly reversed the cytotoxic effect induced by ciclopirox, suggesting that DHX15 is a crucial downstream sensing molecule in response to ciclopirox. Our data therefore suggest a targeting approach of modulating splicing catalysis by repressing DHX15 in T-ALL.

Discussion

Eukaryotic cells can fine-tune gene expression through a variety of mechanisms, in which many co- and post-transcriptional processes are coordinated by RBP.[47,48] Given the pivotal role of these proteins in gene regulatory events, alterations of RBP expression and activity underlie many pathological conditions, including cancer.[49] In this study, we show that the RNA helicase DHX15, transcriptionally activated by MYB, is required for T-cell leukemogenesis. Disruption of DHX15 resulted in mTORC1 inhibition via al-

tered splicing and downregulation of glutamine transporters. We here delineate a MYB-DHX15-mTORC1 axis in T-ALL that engages in leukemogenesis, and also present a DHX15 signature modulator drug, ciclopirox, which shows strong anti-leukemic effects.

As an RBP with helicase activity, accumulating evidence suggests the pivotal role of DHX15 in RNA splicing.[9] We indeed observed alterations of RNA splicing and gene expression in response to *DHX15* loss in T-ALL. Differential splicing and expression identify mTORC1 as a prominent

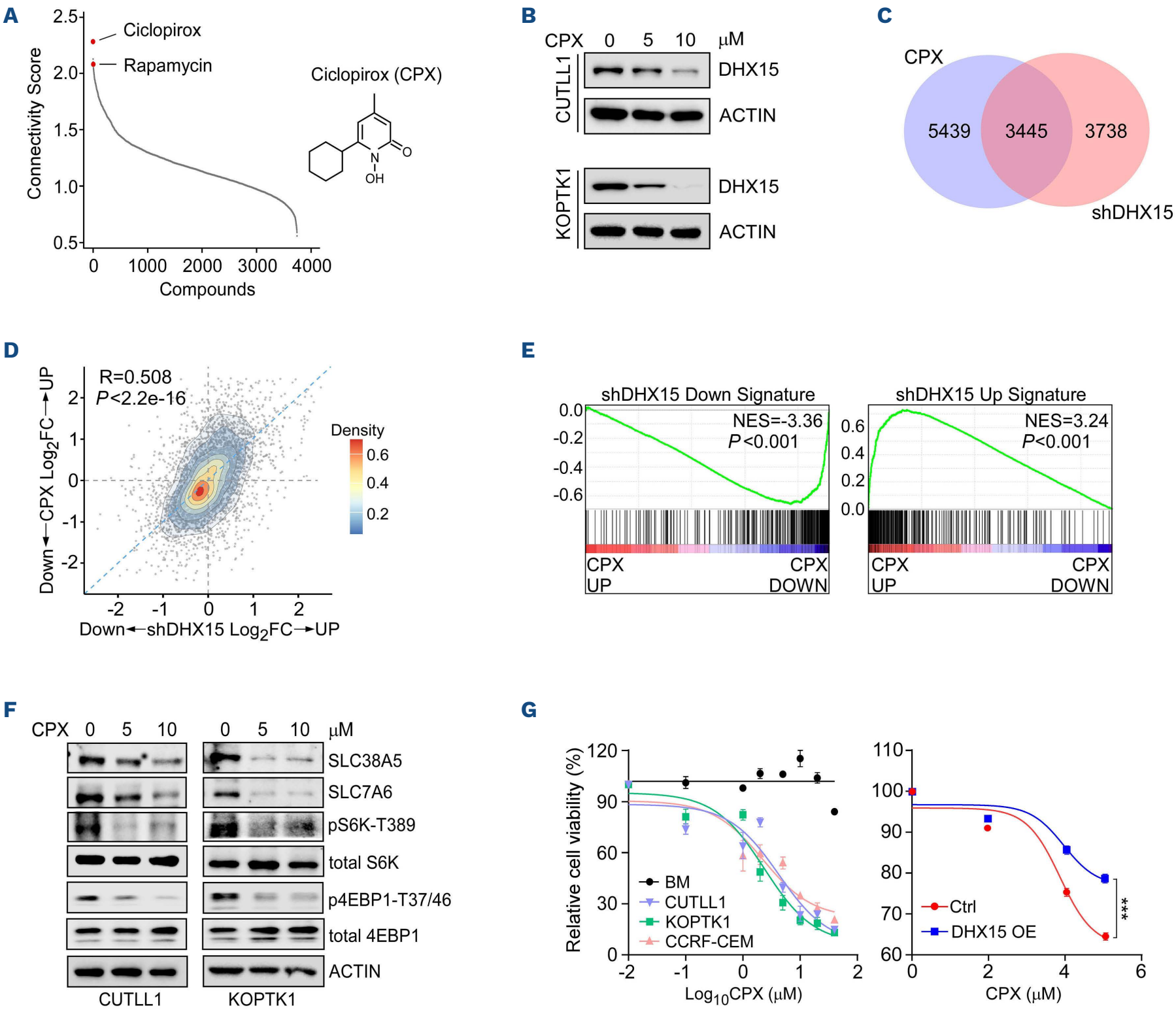

Figure 7. The DHX15 signature modulator drug ciclopirox shows antileukemic effects. (A) Connectivity Map analysis identified ciclopirox (CPX) as the top hit with signatures overlapping those induced by *DHX15* depletion in CUTLL1 cells (left). A gene set consisting of the top 150 upregulated and downregulated genes (P<0.01) was used as input (*www.broad.mit.edu/cmap*). The structure of CPX is shown on the right. (B) Immunoblots of DHX15 in CUTLL1 and KOPTK1 cells treated with CPX for 12 h. (C) Venn diagram showing the overlap between DHX15-regulated and CPX-responsive genes in CUTLL1 cells (P<0.05, fold change >1.3). (D) Density scatter plot showing the correlation of 3,445 overlapping genes indicated in (C) between *DHX15* depletion and CPX exposure. (E) Gene set enrichment analysis of CPX-responsive genes in the expression signature induced by *DHX15* loss (P<0.001, fold change >1.4; top upregulated and downregulated 300 genes). (F) CUTLL1 and KOPTK1 cells were treated with CPX (5 or 10 μM) for 12 h; SLC7A6, SLC38A5, p-S6K T389 and p-4EBP1 T37/46 were analyzed by immunoblot. (G) Analysis of cell viability using the CCK8 Cell Proliferation Assay Kit in T-cell acute lymphoblastic leukemia cells and normal bone marrow cells subjected to CPX treatment for 12 h at various concentrations (left). KOPTK1 cells were infected with lentiviruses expressing ectopic DHX15 (DHX15 OE) or vector control (Ctrl), then subjected to CPX treatment for 12 h at the indicated concentrations. Cell viability was assessed by annexin V-propidium iodide staining and normalized to the untreated control (right). Data shown represent the means (± standard deviation), ***P<0.001. FC: fold change; NES: normalized enrichment score.

DHX15 responsive signaling. The phenotypic consequences of *DHX15* depletion resemble those of mTORC1 inactivation in T-cell lineage that burst proliferation during DN-to-DP transition is profoundly blocked.[38] Our findings thus link DHX15 to mTORC1 signaling as an important mechanism underlying T-cell maturation and T-ALL pathogenesis. Nevertheless, the precise mechanism of how DHX15 dysregulation affects alternative splicing in T-ALL remains to be fully defined.

In contrast to somatic spliceosomal mutations frequently found in myeloid leukemia, such genetic abnormalities are apparently lacking in T-ALL. We previously showed that enhanced SHQ1 expression driven by activating *NOTCH1* mutations modulates snRNA peusdouridylation and regulates RNA splicing,[50] suggesting that lymphoid malignancies may exploit distinct mechanisms for splicing regulation instead of splicing factor somatic mutations. In support of this notion, we here provide further evidence that MYB, overactivated by translocations, duplications and deregulation in T-ALL,[51,52] induces the expression of DHX15, which modulates RNA splicing to enhance the oncogenic mTORC1 pathway. As such, aberrant expression of splicing factors could be a key mechanism underlying oncogenic splicing events and neoplastic phenotypes. Recent reports provide the proof of principle that deubiquitinase USP7, which harbors recurrent genetic mutations in T-ALL, contributes to SRSF6 and SF3B1 stabilization.[22,53] It is therefore reasonable to speculate that T-ALL-specific genetic alterations, exemplified by those found in *NOTCH1, MYB* and *USP7*, govern aberrant expression of splicing factors/modulators. The consequent disordered splicing programs meet the needs for neoplastic transformation, with no necessity of additional spliceosomal mutations.

The widespread splicing changes in human cancers produce pro-tumorigenic isoforms, at the expense of reducing the fidelity of normal splicing function, thus conferring a specific vulnerability to splicing inhibitors. This unique feature propels the development of splicing modulators for the treatment of cancer. Although a number of chemical compounds that modulate splicing catalysis have been described to date, nearly all of these drugs inhibit early spliceosome assembly or SR protein phosphorylation.[7] We here propose clinically approved ciclopirox as a DHX15 signature modulator, thus providing actionable insights toward targeting the late stage of spliceosome disassembly. Supposing that not all introns require the same level of splicing fidelity/complexity, targeting spliceosome disassembly may be less toxic and have more specific effects than inhibiting the early stage of splicing during which the majority of introns are probably affected to some extent. Although the mechanism of action of ciclopirox in regulating DHX15 remains to be determined, these findings suggest novel means of splicing perturbation with clinically available drugs.

Disclosures

No conflicts of interest to disclose.

Contributions

HL and PVV conceived and designed the study. HL, GQ and PVV supervised the study. HL wrote the manuscript. HG and JX performed most of the experiments. PX and ZL conducted the RNA splicing analysis. QL and SP provided technical support. DW analyzed the RNA-sequencing data and performed the Connectivity MAP screen. JL performed RNA immunoprecipitation sequencing and conducted the data analysis. JR, BP, JH, TT and PVV helped to analyze gene expression profiles of primary T-cell and T-acute lymphoblastic leukemia samples. CT and PZ helped to analyze the single-cell RNA sequencing data.

Acknowledgments

We thank members of Liu's, Van Vlierberghe's and Qing's laboratories for helpful suggestions and the Core Facility of the Medical Research Institute at Wuhan University for flow sorting and histological analysis. We are grateful to Dr Jinyong Wang (Guangzhou Institute of Biomedicine and Health, CAS, China) and Dr Haojian Zhang (Wuhan University, China) for providing the Lck-Cre and Mx1-Cre mouse strains. We gratefully acknowledge the Therapeutically Applicable Research to Generate Effective Treatment (TARGET)/Children's Oncology Group (COG), St. Jude Children's Research Hospital and Japan Adult Leukemia Study Group (JALSG) for making their invaluable data available.

Funding

This study was supported by grants from the National Key R&D Program of China (2022YFA1103200), National Natural Science Foundation of China (82161138024, 82025003 and 82011530151 to HL, 81830084 to GQ, 32170565 to ZL), Hubei Provincial Natural Science Fund for Creative Research Groups (2021CFA003 to HL), the Research Foundation Flanders (G0E6222N to PVV) and CAS Hundred Talents Program to ZL.

Data-sharing statement

Raw sequencing data have been deposited in the NCBI Gene Expression Omnibus (GEO) database under accession number GSE208746. Other data supporting the findings of this study are available from the corresponding author, Hudan Liu.

References

1. Yang Q, Jeremiah Bell J, Bhandoola A. T-cell lineage determination. Immunol Rev. 2010;238(1):12-22.
2. Van Vlierberghe P, Ferrando A. The molecular basis of T cell acute lymphoblastic leukemia. J Clin Invest. 2012;122(10):3398-3406.
3. Pui CH, Robison LL, Look AT. Acute lymphoblastic leukaemia. Lancet. 2008;371(9617):1030-1043.
4. Litzow MR, Ferrando AA. How I treat T-cell acute lymphoblastic leukemia in adults. Blood. 2015;126(7):833-841.
5. Cordo V, van der Zwet JCG, Canté-Barrett K, Pieters R, Meijerink JPP. T-cell acute lymphoblastic leukemia: a roadmap to targeted therapies. Blood Cancer Discov. 2021;2(1):19-31.
6. Elcheva IA, Spiegelman VS. Targeting RNA-binding proteins in acute and chronic leukemia. Leukemia. 2021;35(2):360-376.
7. Chen S, Benbarche S, Abdel-Wahab O. Splicing factor mutations in hematologic malignancies. Blood. 2021;138(8):599-612.
8. Lee SC, Abdel-Wahab O. Therapeutic targeting of splicing in cancer. Nat Med. 2016;22(9):976-986.
9. Bohnsack KE, Kanwal N, Bohnsack MT. Prp43/DHX15 exemplify RNA helicase multifunctionality in the gene expression network. Nucleic Acids Res. 2022;50(16):9012-9022.
10. Arenas JE, Abelson JN. Prp43: an RNA helicase-like factor involved in spliceosome disassembly. Proc Natl Acad Sci U S A. 1997;94(22):11798-11802.
11. Tsai RT, Fu RH, Yeh FL, et al. Spliceosome disassembly catalyzed by Prp43 and its associated components Ntr1 and Ntr2. Genes Dev. 2005;19(24):2991-3003.
12. Martin A, Schneider S, Schwer B. Prp43 is an essential RNA-dependent ATPase required for release of lariat-intron from the spliceosome. J Biol Chem. 2002;277(20):17743-17750.
13. Wan R, Yan C, Bai R, Lei J, Shi Y. Structure of an intron lariat spliceosome from Saccharomyces cerevisiae. Cell. 2017;171(1):120-132.
14. Zhang X, Zhan X, Yan C, et al. Structures of the human spliceosomes before and after release of the ligated exon. Cell Res. 2019;29(4):274-285.
15. Ito S, Koso H, Sakamoto K, Watanabe S. RNA helicase DHX15 acts as a tumour suppressor in glioma. Br J Cancer. 2017;117(9):1349-1359.
16. Jing Y, Nguyen MM, Wang D, et al. DHX15 promotes prostate cancer progression by stimulating Siah2-mediated ubiquitination of androgen receptor. Oncogene. 2018;37(5):638-650.
17. Li X, Gounari F, Protopopov A, Khazaie K, von Boehmer H. Oncogenesis of T-ALL and nonmalignant consequences of overexpressing intracellular NOTCH1. J Exp Med. 2008;205(12):2851-2861.
18. Wolf FA, Angerer P, Theis FJ. SCANPY: large-scale single-cell gene expression data analysis. Genome Biol. 2018;19(1):15.
19. Traag VA, Waltman L, van Eck NJ. From Louvain to Leiden: guaranteeing well-connected communities. Sci Rep. 2019;9(1):5233.
20. Van Vlierberghe P, Ambesi-Impiombato A, Perez-Garcia A, et al. ETV6 mutations in early immature human T cell leukemias. J Exp Med. 2011;208(13):2571-2579.
21. Wang E, Lu SX, Pastore A, et al. Targeting an RNA-binding protein network in acute myeloid leukemia. Cancer Cell. 2019;35(3):369-384.
22. Zhou Y, Han C, Wang E, et al. Posttranslational regulation of the exon skipping machinery controls aberrant splicing in leukemia. Cancer Discov. 2020;10(9):1388-1409.
23. Verboom K, Van Loocke W, Volders PJ, et al. A comprehensive inventory of TLX1 controlled long non-coding RNAs in T-cell acute lymphoblastic leukemia through polyA+ and total RNA sequencing. Haematologica. 2018;103(12):e585-e589.
24. Roels J, Kuchmiy A, De Decker M, et al. Distinct and temporary-restricted epigenetic mechanisms regulate human αβ and γδ T cell development. Nat Immunol. 2020;21(10):1280-1292.
25. Homminga I, Pieters R, Langerak AW, et al. Integrated transcript and genome analyses reveal NKX2-1 and MEF2C as potential oncogenes in T cell acute lymphoblastic leukemia. Cancer Cell. 2011;19(4):484-497.
26. Haferlach T, Kohlmann A, Wieczorek L, et al. Clinical utility of microarray-based gene expression profiling in the diagnosis and subclassification of leukemia: report from the International Microarray Innovations in Leukemia Study Group. J Clin Oncol. 2010;28(15):2529-2537.
27. Barretina J, Caponigro G, Stransky N, et al. The Cancer Cell Line Encyclopedia enables predictive modelling of anticancer drug sensitivity. Nature. 2012;483(7391):603-607.
28. Mansour MR, Abraham BJ, Anders L, et al. Oncogene regulation. An oncogenic super-enhancer formed through somatic mutation of a noncoding intergenic element. Science. 2014;346(6215):1373-1377.
29. Biedenkapp H, Borgmeyer U, Sippel AE, Klempnauer KH. Viral myb oncogene encodes a sequence-specific DNA-binding activity. Nature. 1988;335(6193):835-837.
30. Gocho Y, Liu J, Hu J, et al. Network-based systems pharmacology reveals heterogeneity in LCK and BCL2 signaling and therapeutic sensitivity of T-cell acute lymphoblastic leukemia. Nat Cancer. 2021;2(3):284-299.
31. Yang L, Chen F, Zhu H, et al. 3D genome alterations associated with dysregulated HOXA13 expression in high-risk T-lineage acute lymphoblastic leukemia. Nat Commun. 2021;12(1):3708.
32. Zhu H, Dong B, Zhang Y, et al. Integrated genomic analyses identify high-risk factors and actionable targets in T-cell acute lymphoblastic leukemia. Blood Sci. 2022;4(1):16-28.
33. Seki M, Kimura S, Isobe T, et al. Recurrent SPI1 (PU.1) fusions in high-risk pediatric T cell acute lymphoblastic leukemia. Nat Genet. 2017;49(8):1274-1281.
34. Li Y, Li K, Zhu L, et al. Development of double-positive thymocytes at single-cell resolution. Genome Med. 2021;13(1):49.
35. Zhou W, Yui MA, Williams BA, et al. Single-cell analysis reveals regulatory gene expression dynamics leading to lineage commitment in early T cell development. Cell Syst. 2019;9(4):321-337.
36. Zhang J, Huang J, Xu K, et al. DHX15 is involved in SUGP1-mediated RNA missplicing by mutant SF3B1 in cancer. Proc Natl Acad Sci U S A. 2022;119(49):e2216712119.
37. Fingar DC, Richardson CJ, Tee AR, Cheatham L, Tsou C, Blenis J. mTOR controls cell cycle progression through its cell growth effectors S6K1 and 4E-BP1/eukaryotic translation initiation factor 4E. Mol Cell Biol. 2004;24(1):200-216.
38. Hoshii T, Kasada A, Hatakeyama T, et al. Loss of mTOR complex 1 induces developmental blockage in early T-lymphopoiesis and eradicates T-cell acute lymphoblastic leukemia cells. Proc Natl Acad Sci U S A. 2014;111(10):3805-3810.
39. Ma XM, Blenis J. Molecular mechanisms of mTOR-mediated translational control. Nat Rev Mol Cell Biol. 2009;10(5):307-318.
40. Jewell JL, Kim YC, Russell RC, et al. Metabolism. Differential regulation of mTORC1 by leucine and glutamine. Science. 2015;347(6218):194-198.
41. Durán RV, Oppliger W, Robitaille AM, et al. Glutaminolysis activates Rag-mTORC1 signaling. Mol Cell. 2012;47(3):349-358.

42. Garami A, Zwartkruis FJ, Nobukuni T, et al. Insulin activation of Rheb, a mediator of mTOR/S6K/4E-BP signaling, is inhibited by TSC1 and 2. Mol Cell. 2003;11(6):1457-1466.
43. Inoki K, Li Y, Xu T, Guan KL. Rheb GTPase is a direct target of TSC2 GAP activity and regulates mTOR signaling. Genes Dev. 2003;17(15):1829-1834.
44. Ge D, Han L, Huang S, et al. Identification of a novel MTOR activator and discovery of a competing endogenous RNA regulating autophagy in vascular endothelial cells. Autophagy. 2014;10(6):957-971.
45. Subramanian A, Narayan R, Corsello SM, et al. A next generation connectivity map: L1000 platform and the first 1,000,000 profiles. Cell. 2017;171(6):1437-1452.
46. Sehgal VN. Ciclopirox: a new topical pyrodonium antimycotic agent. A double-blind study in superficial dermatomycoses. Br J Dermatol. 1976;95(1):83-88.
47. Glisovic T, Bachorik JL, Yong J, Dreyfuss G. RNA-binding proteins and post-transcriptional gene regulation. FEBS Lett. 2008;582(14):1977-1986.
48. Xiao R, Chen JY, Liang Z, et al. Pervasive chromatin-RNA binding protein interactions enable RNA-based regulation of transcription. Cell. 2019;178(1):107-121.
49. Pereira B, Billaud M, Almeida R. RNA-binding proteins in cancer: old players and new actors. Trends Cancer. 2017;3(7):506-528.
50. Su H, Hu J, Huang L, et al. SHQ1 regulation of RNA splicing is required for T-lymphoblastic leukemia cell survival. Nat Commun. 2018;9(1):4281.
51. Clappier E, Cuccuini W, Kalota A, et al. The C-MYB locus is involved in chromosomal translocation and genomic duplications in human T-cell acute leukemia (T-ALL), the translocation defining a new T-ALL subtype in very young children. Blood. 2007;110(4):1251-1261.
52. Lahortiga I, De Keersmaecker K, Van Vlierberghe P, et al. Duplication of the MYB oncogene in T cell acute lymphoblastic leukemia. Nat Genet. 2007;39(5):593-595.
53. Han C, Khodadadi-Jamayran A, Lorch AH, et al. SF3B1 homeostasis is critical for survival and therapeutic response in T cell leukemia. Sci Adv. 2022;8(3):eabj8357.